Environmental Gas and Light Sensing Using ZnO Nanowires

Nima Mohseni Kiasari, Saeid Soltanian, Bobak Gholamkhass, and Peyman Servati, *Member, IEEE*

***Abstract*—In this paper, vertical arrays of zinc oxide (ZnO) nanowires (NWs) are synthesized by a chemical vapor deposition system and then deposited on patterned electrodes using dielectrophoresis. The NW devices illustrate four orders of magnitude increase in conductivity when exposed to ultraviolet (UV) irradiation of 1220 μW/cm^2. UV response has a fast component, due to electron-hole generation, as well as a slower component, attributed to the release of oxygen species from the surface of NW. Moreover, due to the increased electron density in the presence of UV, the type of oxygen species on the surface of ZnO changes to more reactive negative ions. In addition, when the pressure is decreased to 0.05 mBar, the conductivity of the NWs increases $\sim$3.5 times due to the removal of oxygen molecules from the surface. For the first time, UV irradiation is used to improve the carbon monoxide (CO) sensing properties of ZnO NWs. When exposed to 250 μW/cm^2 UV irradiation, not only the sensitivity increases more than 75%, but also a repeatable and recoverable response is obtained, which is due to formation of more reactive oxygen ions. For the same reason, when the temperature is elevated, higher sensitivity to CO is achieved. The devices demonstrate exponential sensitivities of more than four decades when the relative humidity (RH) increases to 86% at room temperature.**

***Index Terms*—Carbon monoxide (CO) sensing, UV activated sensing, dielectrophoresis (DEP), gas sensor, oxygen, relative humidity (RH), ultraviolet (UV) detector, zinc oxide (ZnO) nanowire (NW).**

I. Introduction

MONITORING and control of environmental parameters such as humidity, oxygen concentration, light intensity, and air pollutants is essential for improving the quality of life and refining manufacturing and operational processes in automotive, medical, and semiconductor industries. With the emerging demands for fast, accurate, low-cost, and ubiquitous sensing of these parameters, small footprint and low-cost sensors based on zinc oxide (ZnO) nanostructures have become attractive. The simplicity, variety, and low-cost of synthesis methods (e.g., chemical vapor deposition (CVD), laser ablation, hydrothermal, and sol–gel processes) as well as the morphological diversity (e.g., nanoparticles, nanowires (NWs), nanorods, nanobelts, and tetrapods) have made ZnO an appealing candidate for sensing applications. Owing to the high surface-to-volume ratio of nanostructures as well as the surficial oxygen vacancies, ZnO nanosensors are highly sensitive to various environmental parameters such as concentrations of oxygen [1]–[5], carbon monoxide (CO) [3], relative humidity (RH) [6]–[9], hydrogen [10], and ultraviolet (UV) irradiation [11].

Scalable integration of these nanostructures, in particular NWs, into electronic devices, as the active component, still remains as a challenge. Conventional fabrication processes for making metallic contacts to the NWs involve sophisticated photolithography, electron-beam lithography or focused ion beam, which hinder the commercial development of NW-based devices. In recent years, dielectrophoresis (DEP) [12], [13] has shown to be a powerful, low cost, scalable and yet high-yield alternative for assembly of NW devices.

Despite several reports on sensing applications of ZnO NWs [3], [6], [14]–[16], there has not been a thorough study on various aspects of ZnO NW's sensitive nature, as most of the published articles only focus on the response of sensors to a specific type of stimulus. In this paper, a comprehensive study is presented for the sensing properties of DEP-assembled devices, in response to different intensities of UV irradiation and varying concentrations of oxygen, RH, CO, and vacuum levels. Moreover, not only the effect of UV irradiation on sensing behavior to each of these stimuli is examined but also the correlation between UV and RH as well as hydrostatic pressure is systematically studied. We believe this comprehensive study not only increases our knowledge about the science behind the sensing mechanism of the ZnO NWs but also paves the way for addressing the selectivity issue of the metal oxide sensors.

II. Experimental Details

A. NW Synthesis and Characterization

Synthesis of NWs was carried out in a horizontal tube of a CVD system. The NWs were grown on a (1 0 0) silicon wafer coated with a 100 nm thermally evaporated gold layer as substrate. Equal molar ratios of ZnO (99.999%, Alfa Aesar) and graphite powder (99.9%, Alfa Aesar) were used as the precursor for NW growth. Horizontal tube furnace was heated up to 950 °C and then a quartz boat containing the precursor mixture and silicon growth substrates was loaded inside the furnace in such a way that the source material was located in the middle of the hot zone and the silicon substrates at 12–14 cm far from the source on downstream ($\sim$800 °C). Furnace is connected to a vacuum pump that maintains the pressure level inside the tube at $\sim$1 mbar under a constant flow of 30 standard cubic

Manuscript received October 15, 2013; revised January 28, 2014; accepted February 4, 2014. Date of publication February 20, 2014; date of current version March 6, 2014. The review of this paper was arranged by Associate Editor J. Li.

The authors are with the Department of Electrical and Computer Engineering, University of British Columbia, Vancouver, BC V6T 1Z4 USA (e-mail: nimamk@ece.ubc.ca; Saeid@ece.ubc.ca; bobgk@ece.ubc.ca; peymans@ece.ubc.ca).

Color versions of one or more of the figures in this paper are available online at http://ieeexplore.ieee.org.

Digital Object Identifier 10.1109/TNANO.2014.2305621

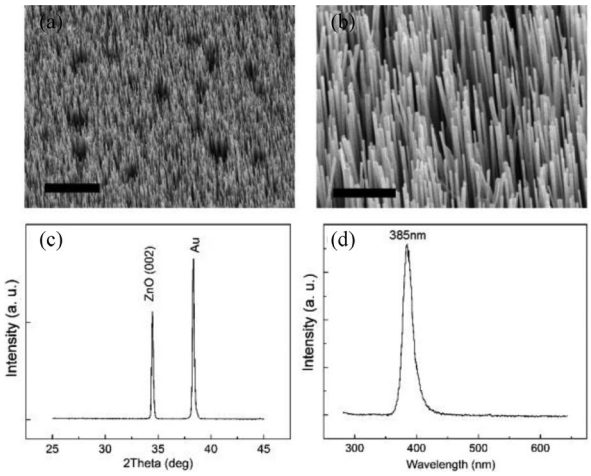

Fig. 1. (a) Low and (b) high magnification 45°-titled SEM micrograph of vertically aligned ZnO NWs (scale bar is 10 and 2 μm for a and b, respectively), and (c) XRD pattern and (c) PL spectrum of the synthesized ZnO NWs.

centimeters per minute comprising 90% Ar and 10% oxygen. The growth process takes 2–3 h depending on the desired length of the NWs. The as-grown NW arrays were characterized by scanning electron microscope (SEM), X-ray diffraction (XRD), and photoluminescence (PL) spectroscopy. Fig. 1(a) illustrates a typical 45° tilted SEM micrograph of the synthesized ZnO NW arrays, showing a high density of vertically aligned NWs grown uniformly, and Fig. 1(b) displays a higher magnification SEM image confirming NWs with diameter of 80–130 nm and an approximate density of $\sim$25 NW/μm^2. In addition, the strong intensity of ZnO (0 0 2) diffraction peak [see Fig. 1(c)] confirms a vertical alignment of the single crystalline NWs. The photoluminescense properties of ZnO NW arrays were also examined at room temperature using a pulsed laser (35 ps pulse duration and 10 Hz repetition rate) with excitation wavelength of 266 nm and intensity of 5 mW/cm^2. As shown in Fig. 1(d), a narrow band ultraviolet (UV) emission was observed in PL spectra at the wavelength of about 385 nm that is attributed to the near band edge transition of ZnO NWs.

B. Device Fabrication

A 25-mm^2 substrate onto which the NWs were grown was ultrasonicated (using a bath ultrasonic) in 2 mL of ethanol for a few seconds to detach the NWs from the substrate and disperse them in ethanol. N-type Si (100) wafers with 300-nm thermally grown silicon oxide were used as the substrate for device fabrication. Micropatterned gold electrodes (100-nm thick and 3-μm channel width) were developed by standard photolithography and lift-off process. ZnO NWs were then deposited between micropatterned gold electrodes using DEP by dropping 5 μL of NW suspension in ethanol and applying a sine voltage with amplitude of 10 V and frequency of 0.5 MHz for 2 min. These values for amplitude and frequency were tuned based on the gap size and NW concentration in the solution in order to obtain the highest probability for capturing NWs in the gap. The ac signal generates an alternating electric field in the gap between gold electrodes and induces a dipole in ZnO NW so that the polarized NW is attracted toward electrode gap under a high electric field gradient [9]. The inset in Fig. 2 shows SEM micrographs of a device after DEP and capturing of NWs between metallic electrodes.

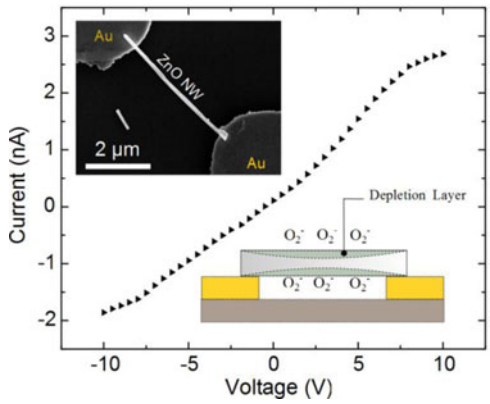

Fig. 2. Current–voltage characteristic of a typical ZnO sensor. A DEP-assembled device with an NW captured between two gold electrode as well as the schematics of an NW aligned across two metallic electrodes are shown in the insets.

Fig. 2 illustrates a typical current–voltage characteristic of a ZnO device at room temperature. As observed, the device shows a resistive behavior with a relatively good Ohmic behavior for the applied voltage range of -10–10 V.

The fabricated devices were wire bonded to a printed circuit board and placed in a custom made aluminum environmental chamber electrically wired to a semiconductor characterization system (Keithley 4200-SCS). The chamber was connected to a gas mixer controlled with fully controlled mass flow controllers (MKS 1179) and a digital readout (CCR 400A) run by a computer. Moreover, the chamber as well as the tubes and fittings were wrapped with heating tape connected to a temperature controller equipped with a K-type thermocouple. The steady state as well as transient current–voltage characteristics were systematically measured and investigated under various conditions described in the following sections.

III. Results and Discussion

A. Ultraviolet (UV) Light Detection

ZnO has a wide band gap ($\sim$3.3 eV [17]) and as shown in the PL results in Fig. 1(d), the observed UV emission wavelength of 385 nm at room temperature corresponds to this band gap energy. Fig. 3(a) illustrates the sensitivity of the current–voltage characteristics of the ZnO NWs to different intensities (from 0 to 1220 μW/cm^2) of UV irradiation (peak intensity $\lambda_{\max}$ of 365 nm). The intensity of the incident UV irradiation was measured separately using a photodetector (Newport 818-UV). As shown in the figure, under UV illumination, carriers are generated by a band-to-band transition, resulting in the observed dramatic increase in the current [11], [18], [19]. For instance, a UV intensity of 1220 μW/cm^2 increases the electrical current by more than four and Y. Li *et al.* [20], can be attributed to the low carrier density under dark conditions due to the oxygen rich CVD synthesis of our NWs [9]. Fig. 3(b) depicts the transient

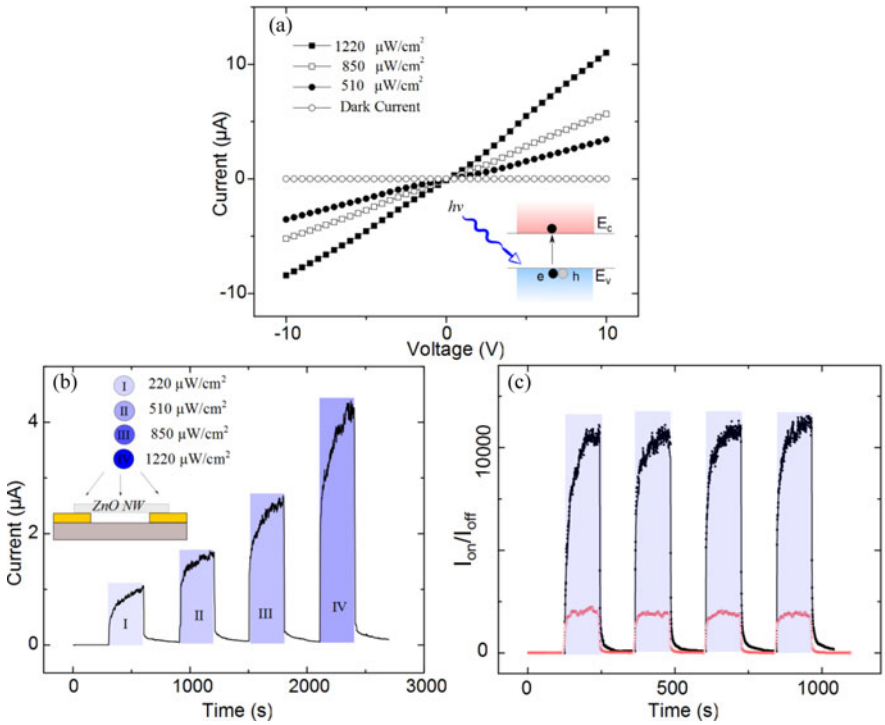

Fig. 3. (a) Current–voltage characteristics of the sensor under UV illumination with different intensities (at room temperature). The transient response of the sensor to (b) the UV pulses with different intensities, and (c) four successive UV pulses with the same intensity (1220 μW/cm^2: black, and five times attenuated: red).

response of the sensor to the UV irradiation pulses (300 s) with different intensities, showing the scaling of the current with the pulse intensity. Fig. 3(c) demonstrates the transient response of the sensor normalized to dark current to four pulses (120 s) of UV with the same intensity 1220 μW/cm^2 (and also for five times attenuated intensity of 250 μW/cm^2), signifying the repeatability of the response. As observed from these two figures, the sensors demonstrate fast and repeatable transient responses to UV pulses with a response time (10% to 90% of final value) of $\sim$38 s and a recovery time (90% to 10%) of 12 s for the maximum intensity (1220 μW/cm^2). For the 20% intensity, the response and recovery times are 21 and 6 s, respectively.

The UV responses of the sensors are tested at the atmospheric and reduced pressures by placing the devices in a vacuum chamber connected to a semiconductor analyzer. To ensure the removal of humidity, the chamber is purged and refilled with the dry air ($H_2O < 10$ ppm). As seen in the inset of Fig. 4, the resistance of the sensor under dark condition decreases as the pressure reduces, due to the desorption of previously chemisorbed oxygen species [1] from the surface of NWs that leads to release of electrons contributing to improved conduction in the NW. Fig. 4 illustrates the transient response of the sensor to a UV pulse (180 s) at the atmospheric and 0.005 mbar pressures. Although the device shows similar photocurrents under both pressure levels, it exhibits different recovery behaviors. It is deduced that the response and recovery of a ZnO NW to UV light is not solely due to bulk generation and recombination processes. Under UV irradiation the release of oxygen molecules from the surface can occur due to the migration of holes toward the surface and reaction with the negatively charged chemisorbed oxygen species ($h^+ + O_2^- \rightarrow O_2$) [21]. As a result, when the UV is turned OFF, while the majority of electrons and holes recombine rapidly, a residual electron population associated to the released oxygen molecules will remain until oxygen is reabsorbed on the surface [21]–[23]. As expected this recovery is dramatically slow under vacuum conditions in comparison to the atmospheric pressure. The same behavior, slower recovery under vacuum, is also observed previously [22], [23].

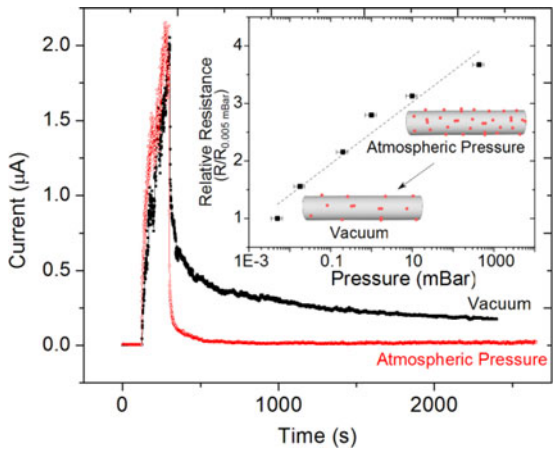

Fig. 4. Transient response of the sensor to a 180-s UV pulse under atmospheric versus reduced pressure at room temperature. The inset shows the resistance of the sensor as a function of pressure under dark conditions.

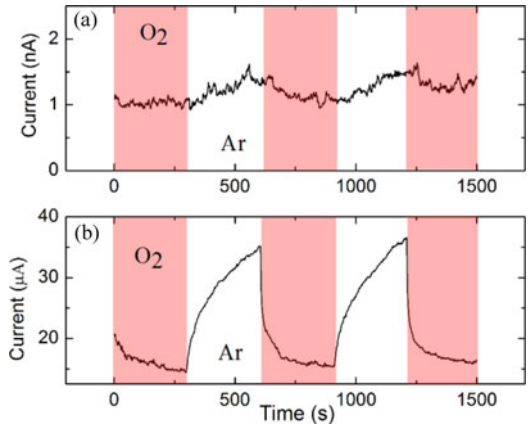

Fig. 5. Time transient behavior of the ZnO sensor to pulses of oxygen and argon (a) under dark and (b) under UV irradiation at room temperature.

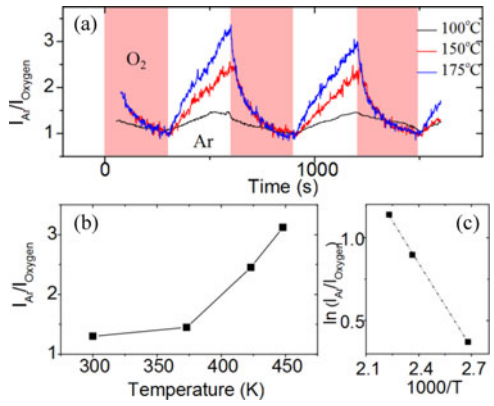

Fig. 6. (a) Time transient response of the sensor to successive pulses of oxygen and argon at different temperatures. (b) Sensitivity as a function of temperature. (c) Arrhenius plot of the sensor's response.

B. Oxygen Sensing

In addition to sensitivity to vacuum, adsorption and desorption of oxygen on the surface of the NW can be used for sensing the oxygen content of the ambient. Fig. 5 displays the response of a ZnO NW sensor to repetitive pulses (300-s long) of pure oxygen and argon in the dark and under UV irradiation. As observed, the sensor response is weak in the dark, since the surface of NW is highly saturated with oxygen. However, once the sensor is under UV irradiation, the current of the sensor changes about 250% when the surrounding oxygen atmosphere is replaced with argon. The influence of light irradiating on gas sensing properties of metal oxides has been reported in the literature [24]–[27]. The pronounced sensitivity to oxygen affirms our previous discussion that the UV illumination facilitates removal of some chemisorbed oxygen species, thus increasing sensitivity to oxygen in the ambient. In particular, UV irradiation forms weakly bound photoinduced oxygen ions [28], which require less energy for desorption at room temperature.

Thermal energy can be used to overcome the energy barrier of oxygen adsorption and desorption instead of UV irradiation [29]. Fig. 6 displays the transient response of the ZnO NWs to pulses of oxygen and argon at different temperatures (100, 150, and 175 °C). The increased sensitivity at higher temperatures can be attributed to the increased surface activity as well as the additional role of some reactive oxygen species that occur at higher temperatures [1]. It is known that at room temperature, an oxygen molecule accepts one electron from the NW to forms O_2^-. However, at temperatures higher than 100 °C, the oxygen molecule dissociates and accepts another electron to form 2 O^- [30]. From the Arrhenius plot, the activation energy of this reaction is estimated to be 146 meV for pure oxygen ambient for 100 °C $< T <$ 200 °C [31].

C. RH Sensing

The steady state and transient responses of the ZnO NWs are investigated under humidified air with controlled RH as monitored by an independent digital humidity meter (TPI 597) connected to the test chamber. As shown in Fig. 7(a), the conductivity of the ZnO NW is improved significantly with an increasing RH (i.e., more than four orders of magnitude change in current when the ambient changes from dry to 86% RH). Although it has been widely known that water molecules can dissociate and donate electrons to ZnO through a chemisorption process, this usually requires a high energy and does not happen at temperatures below 100 °C [32]. As we demonstrated in our previous study [9], the mechanism responsible for the observed change in the conductivity at room temperature is the replacement of the initial oxygen species on the NW surface [30] with physisorbed water molecules. This replacement leads to release of electrons in the NW and increased conductivity.

In the inset of Fig. 7(a), the transient response of the sensor to 86% RH pulses is shown, which signifies a fast, and repeatable response. Fig. 7(b) illustrates the transient response of the sensor to step-like changes of RH from dry to 86% (10-min long steps) showing a stable operation at room temperature.

Fig. 8 depicts the correlation of the effect of UV and RH on the sensor response. The transient response to the successive pulses of 80% RH air and dry air under both dark and UV irradiation conditions is shown in Fig. 8(a). In contrast, Fig. 8(b) demonstrates the response to UV pulses under dry and 80% RH conditions. From these two measurements, it is observed that not only the sensitivity to RH drops in the presence of UV but also the sensitivity to UV diminishes substantially in the presence of humidity. For example, the sensor's sensitivity to 80% RH pulses with respect to dry air decreases from 8000 to 3.5 under UV irradiation. Similarly, the sensitivity to the UV pulses drops from 2000 to 5 in an 80% RH ambient.

As mentioned earlier, both UV and humidity lead to an increased number of carriers. As a result, in the presence of UV or humidity, the sensitivity to the other is lower due to the existing carriers in the NW.

D. CO Sensing

Fig. 9 demonstrates the transient responses of ZnO NW sensors to pulses of CO. Oxygen species on the surface of NW can react with CO to form carbon dioxide and release an electron in the NW. Similar to previous studies [3], [29], [33], at room temperature and under dark conditions, the sensitivity of the sensor to pure CO gas is low, as shown in Fig. 9(a). However,

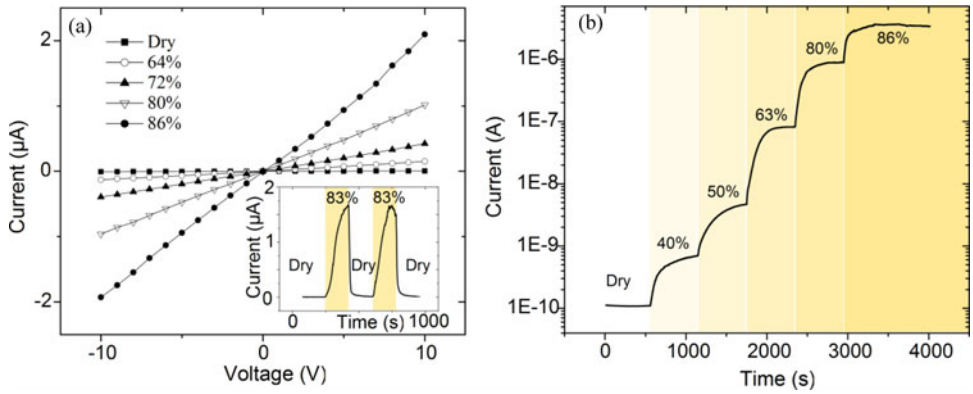

Fig. 7. (a) Steady state $I-V$ characteristic of the ZnO sensor under various RH levels at room temperature. The inset shows the transient response to pulses of 86% RH between dry air purges. (b) Transient response of the sensor to increasing RH from dry to 86%.

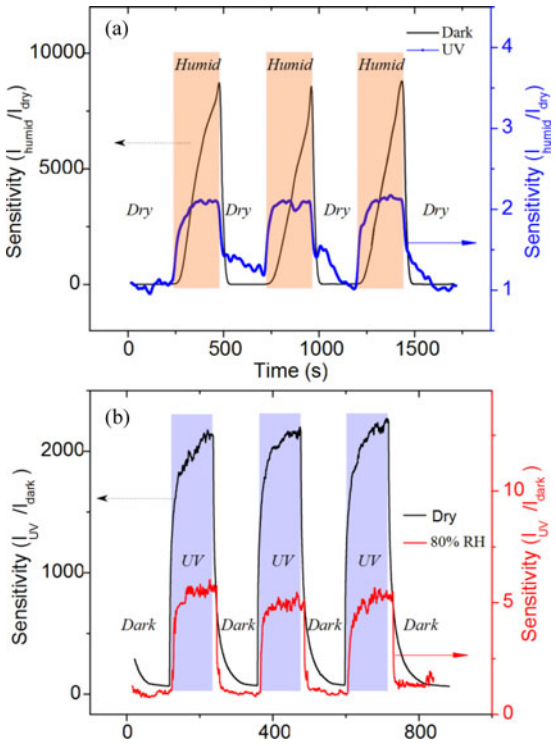

Fig. 8. Transient response of the sensor at room temperature to (a) the successive 80% RH air and dry air pulses under dark and UV irradiation, and (b) the successive UV pulses in the dry and 80% RH air ambient.

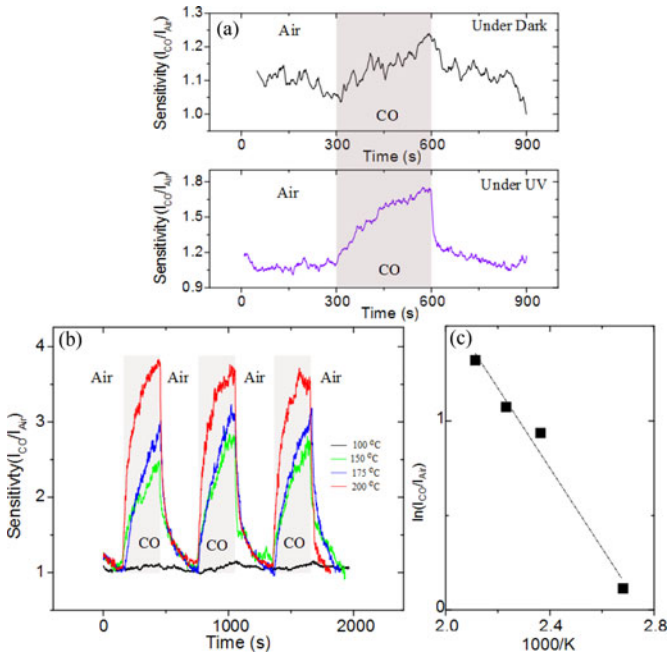

Fig. 9. Transient response of the sensor to (a) pulses of pure CO and air under dark and UV irradiation conditions, and (b) the successive 5-min-long CO and air pulses at different ambient temperatures (100, 150, 175, and 200 °C). (c) Arrhenius plot of the sensitivity of the NW sensor to pure CO.

under UV irradiation, the sensitivity increases to 75% due to the formation of reactive photoinduced oxygen ions on the surface of the NW [28]. The improvement in the sensitivity, however, is not as remarkable as the case of oxygen. This difference can be attributed to the partial release of the chemisorbed oxygen species from the surface of the NWs under UV irradiation [21], which is not desirable for CO sensing. Fig. 9(b) illustrates the sensitivity of the ZnO sensor to the CO pulses at different ambient temperatures (i.e., 100, 150, 175, and 200 °C). As seen, at elevated temperatures, the sensitivity significantly improves due to the enhanced surface activity similar to the case of oxygen. In addition, as reported by Takata *et al.* [30], at temperatures below 100 °C, the dominant reactive oxygen ions are O_2^-, as compared to the more reactive O^- species at temperatures between 100 and 300 °C [34].

Fig. 9(c) depicts the Arrhenius plot of the sensitivity to pure CO, signifying a linear behavior in agreement with the thermionic emission model [5]. An effective activation energy *Ea* of 180 meV for pure CO ambient can be extracted (slope $=$ Ea/k_B, where k_B is the Boltzmann constant) for 100 °C $< T <$ 200 °C.

Fig. 10 shows the transient response of the sensor at 200 °C ambient temperature to the successive pulses of air having different concentrations of CO (i.e., 10%, 20%, ... 100%), which displays a monotonic dependence of the current to the concentration of CO. When the CO percentage varies from 10% to 100% the response times vary from 50 to 160 s, respectively, showing a slower response at larger changes in the concentrations of CO.

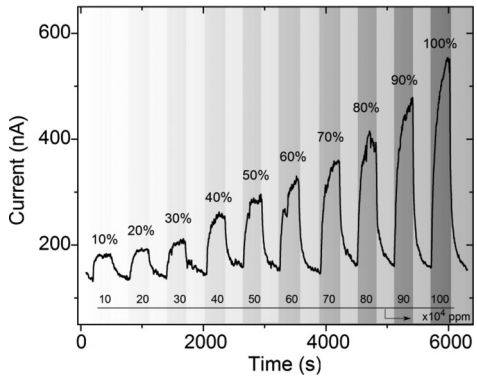

Fig. 10. Transient response of the sensor to the successive pulses of air having different concentrations of CO from 10% to 100% at 200 °C.

However, the recovery times remain almost independent of the CO concentration and between 87 and 97 s.

IV. Conclusion

We have shown a low-cost and convenient way for fabricating high-performance environmental sensors based on CVD grown single-crystalline ZnO NWs. The fabricated devices exhibit more than four orders of magnitude change in conductivity when exposed to UV light with the power density of 1220 μW/cm^2. It was shown that the change in conductivity of ZnO NW is not only due to EHP generation but also release of negatively charged oxygen species from the surface of NWs. Also the resistance increases more than three times when the sensor is exposed to pure oxygen ambient at 175 °C and four times improvement in conductivity when exposed to CO ambient at 200 °C. The sensors also illustrate exponential change in excess of four decades in response to 85% RH air at room temperature. In addition, these devices displayed improved sensitivity to oxygen and CO when exposed to UV illumination due to the formation of weakly bound photoinduced oxygen species at the surface of the NW. It was noticed that not only the sensitivity to RH drops in the presence of UV but also the sensitivity to UV diminishes substantially in the presence of humidity.

Acknowledgment

The authors would like to acknowledge the financial support of the Natural Sciences and Engineering Research Council of Canada, Canada Foundation for Innovation, and MITACS. They also thank Y. Wang for SEM imaging and L. Chrostowski for using his lab facilities for measuring the UV power density and spectrum.

References

[1] N. M. Kiasari and P. Servati, "Dielectrophoresis-assembled ZnO nanowire oxygen sensors," *IEEE Electron Device Lett.*, vol. 32, no. 7, pp. 982–984, Jul. 2011.

[2] Q. Li, Y. Liang, Q. Wan, and T. Wang, "Oxygen sensing characteristics of individual ZnO nanowire transistors," *Appl. Phys. Lett.*, vol. 85, pp. 6389–6391, 2004.

[3] S. J. Chang, T. J. Hsueh, I. C. Chen, and B. R. Huang, "Highly sensitive ZnO nanowire CO sensors with the adsorption of Au nanoparticles," *Nanotechnology*, vol. 19, p. 175502, 2008.

[4] N. M. Kiasari, S. Soltanian, B. Gholamkhass, and P. Servati, "Low cost environmental sensors using zinc oxide nanowires and nanostructures," *MRS Online Proc. Library*, vol. 1439, 2012.

[5] Z. Fan, D. Wang, P.-C. Chang, W.-Y. Tseng, and J. G. Lu, "ZnO nanowire field-effect transistor and oxygen sensing property," *Appl. Phys. Lett.*, vol. 85, p. 5923, 2004.

[6] S. P. Chang, S. J. Chang, C. Y. Lu, M. J. Li, C. L. Hsu, Y. Z. Chiou, T. J. Hsueh, and I. Chen, "A ZnO nanowire-based humidity sensor," *Superlattices Microstruct.*, vol. 47, pp. 772–778, 2010.

[7] B. M. Kulwicki, "Humidity sensors," *J. Amer. Ceramic Soc.*, vol. 74, pp. 697–708, 1991.

[8] Q. Qi, T. Zhang, Q. Yu, R. Wang, Y. Zeng, L. Liu, and H. Yang, "Properties of humidity sensing ZnO nanorods-base sensor fabricated by screen-printing," *Sens. Actuators B: Chemical*, vol. 133, pp. 638–643, 2008.

[9] N. M. Kiasari, S. Soltanian, B. Gholamkhass, and P. Servati, "Room temperature ultra-sensitive resistive humidity sensor based on single zinc oxide nanowire," *Sens. Actuators A: Phys.*, vol. 182, pp. 101–105, 2012.

[10] H. T. Wang, B. Kang, F. Ren, L. Tien, P. Sadik, D. Norton, S. Pearton, and J. Lin, "Hydrogen-selective sensing at room temperature with ZnO nanorods," *Appl. Phys. Lett.*, vol. 86, p. 243503, 2005.

[11] C. Soci, A. Zhang, B. Xiang, S. Dayeh, D. Aplin, J. Park, X. Bao, Y. Lo, and D. Wang, "ZnO nanowire UV photodetectors with high internal gain," *Nano Lett.*, vol. 7, pp. 1003–1009, 2007.

[12] E. M. Freer, O. Grachev, X. Duan, S. Martin, and D. P. Stumbo, "High-yield self-limiting single-nanowire assembly with dielectrophoresis," *Nature Nanotechnol.*, vol. 5, pp. 525–530, 2010.

[13] A. Kashefian Naieni and A. Nojeh, "Effect of solution conductivity and electrode shape on the deposition of carbon nanotubes from solution using dielectrophoresis," *Nanotechnology*, vol. 23, p. 495606, 2012.

[14] S. J. Chang, W. Y. Weng, C. L. Hsu, and T. J. Hsueh, "High sensitivity of a ZnO nanowire-based ammonia gas sensor with Pt nano-particles," *Nano Commun. Netw.*, vol. 1, pp. 283–288, 2010.

[15] Q. Wan, Q. Li, Y. Chen, T. Wang, X. He, J. Li, and C. Lin, "Fabrication and ethanol sensing characteristics of ZnO nanowire gas sensors," *Appl. Phys. Lett.*, vol. 84, p. 3654, 2004.

[16] S. J. Chang, T. J. Hsueh, C. L. Hsu, Y. R. Lin, I. C. Chen, and B. R. Huang, "A ZnO nanowire vacuum pressure sensor," *Nanotechnology*, vol. 19, p. 095505, 2008.

[17] F. Shan and Y. Yu, "Band gap energy of pure and Al-doped ZnO thin films," *J. Eur. Ceramic Soc.*, vol. 24, pp. 1869–1872, 2004.

[18] T. H. Moon, M. C. Jeong, W. Lee, and J. M. Myoung, "The fabrication and characterization of ZnO UV detector," *Appl. Surface Sci.*, vol. 240, pp. 280–285, 2005.

[19] J. Zhou, Y. Gu, Y. Hu, W. Mai, P. H. Yeh, G. Bao, A. K. Sood, D. L. Polla, and Z. L. Wang, "Gigantic enhancement in response and reset time of ZnO UV nanosensor by utilizing Schottky contact and surface functionalization," *Appl. Phys. Lett.*, vol. 94, p. 191103, 2009.

[20] Y. Li, F. Della Valle, M. Simonnet, I. Yamada, and J.-J. Delaunay, "High-performance UV detector made of ultra-long ZnO bridging nanowires," *Nanotechnology*, vol. 20, p. 045501, 2009.

[21] D. A. Melnick, "Zinc oxide photoconduction, an oxygen adsorption process," *J. Chemical Phys.*, vol. 26, p. 1136, 1957.

[22] Q. Li, T. Gao, Y. Wang, and T. Wang, "Adsorption and desorption of oxygen probed from ZnO nanowire films by photocurrent measurements," *Appl. Phys. Lett.*, vol. 86, p. 123117, 2005.

[23] Q. Li, Q. Wan, Y. Liang, and T. Wang, "Electronic transport through individual ZnO nanowires," *Appl. Phys. Lett.*, vol. 84, pp. 4556–4558, 2004.

[24] T.-Y. Yang, H.-M. Lin, B.-Y. Wei, C.-Y. Wu, and C.-K. Lin, "UV enhancement of the gas sensing properties of nano-TiO2," *Rev. Adv. Mater. Sci*, vol. 4, pp. 48–54, 2003.

[25] A. Soleimanpour, S. V. Khare, and A. H. Jayatissa, "Enhancement of hydrogen gas sensing of nanocrystalline nickel oxide by pulsed-laser irradiation," *ACS Appl. Mater. Interfaces*, vol. 4, pp. 4651–4657, 2012.

[26] E. Comini, A. Cristalli, G. Faglia, and G. Sberveglieri, "Light enhanced gas sensing properties of indium oxide and tin dioxide sensors," *Sens. Actuators B: Chemical*, vol. 65, pp. 260–263, 2000.

[27] S.-W. Fan, A. K. Srivastava, and V. P. Dravid, "UV-activated room-temperature gas sensing mechanism of polycrystalline ZnO," *Appl. Phys. Lett.*, vol. 95, p. 142106, 2009.

[28] T. Barry and F. Stone, "The reactions of oxygen at dark and irradiated zinc oxide surface," in *Proc. Roy. Soc. London. Series A. Math. Phys. Sci.*, 1960, vol. 255, pp. 124–144.
[29] J. Chang, H. Kuo, I. Leu, and M. Hon, "The effects of thickness and operation temperature on ZnO: Al thin film CO gas sensor," *Sens. Actuators B: Chemical*, vol. 84, pp. 258–264, 2002.
[30] M. Takata, D. Tsubone, and H. Yanagida, "Dependence of electrical conductivity of ZnO on degree of sintering," *J. Amer. Ceramic Soc.*, vol. 59, pp. 4–8, 1976.
[31] P. Clifford and D. Tuma, "Characteristics of semiconductor gas sensors II. Transient response to temperature change," *Sens. Actuators*, vol. 3, pp. 255–281, 1983.
[32] Z. Chen and C. Lu, "Humidity sensors: A review of materials and mechanisms," *Sens. Lett.*, vol. 3, pp. 274–295, 2005.
[33] R. K. Joshi, Q. Hu, F. Alvi, N. Joshi, and A. Kumar, "Au decorated zinc oxide nanowires for CO sensing," *J. Phys. Chemistry. C, Nanomat. Interfaces*, vol. 113, p. 16199, 2009.
[34] S. R. Morrison, "Mechanism of semiconductor gas sensor operation," *Sens. Actuators*, vol. 11, pp. 283–287, 1987.

Authors' photographs and biographies not available at the time of publication.